Tellus
SERIES B
CHEMICAL
AND PHYSICAL
METEOROLOGY
PUBLISHED BY THE INTERNATIONAL METEOROLOGICAL INSTITUTE IN STOCKHOLM

Tellus (2011), 63B, 64–76

Atmospheric molecular hydrogen (H_2): observations at the high-altitude site Jungfraujoch, Switzerland

By S.W. BOND*, M.K. VOLLMER, M. STEINBACHER, S. HENNE and S. REIMANN,
Empa, Swiss Federal Laboratories for Materials Science and Technology, Laboratory for Air Pollution/Environmental Technology, Ueberlandstrasse 129, CH-8600 Duebendorf, Switzerland

(Manuscript received 4 February 2010; in final form 6 September 2010)

ABSTRACT

Measurements of H_2 at the high-altitude site of Jungfraujoch, Switzerland are reported upon for the period of August, 2005–November, 2009. The time series consists of measurements that are primarily representative of free tropospheric background conditions. Highest background H_2 mixing ratios were observed in May, while the lowest were observed in November. The mean seasonal H_2 peak-to-trough amplitude of 21 parts per billion (ppb, 10^{-9} dry air mixing ratio) at Jungfraujoch was considerably less than at other stations at similar latitudes and the seasonal minimum in November was comparatively delayed. These differences are primarily attributed to a dampening and delay of the surface soil sink signal during its vertical propagation to the free troposphere. Excess (mixing ratio minus corresponding baseline value) H_2 (ΔH_2) and excess CO (ΔCO) displayed no significant correlation. This lacking correlation is attributed to H_2 removal by soil during transport to Jungfraujoch, thereby significantly altering the $\Delta H_2/\Delta$CO ratio from traffic combustion sources, which is the largest source of anthropogenic H_2 influencing measurements at Jungfraujoch.

1. Introduction

Atmospheric molecular hydrogen (H_2) has received increased attention recently due to its potential as a sustainable energy carrier and fuel source for transportation, along with the possible environmental consequences that may accompany its large-scale adoption. An increase in tropospheric H_2 could lead to a reduction of the atmosphere's oxidizing capacity, primarily through the reduction of hydroxyl radicals (OH), which would consequently increase the lifetime of methane (CH_4) in the atmosphere (H_2 and CH_4 similarly compete for the oxidizing OH radical), thereby increasing the radiative forcing of CH_4 (Schultz et al., 2003). In addition, an increase in the atmospheric H_2 burden could favour the production of tropospheric ozone (O_3) due to changes in tropospheric OH radical concentrations (Hauglustaine and Ehhalt, 2002). Derwent et al. (2006) found that through these interactions, H_2 can be considered an indirect greenhouse gas with an indirect global warming potential of 5.8 over a 100-yr time horizon, which is low compared with most other radiatively active trace gases. An increase in atmospheric H_2 has also been implicated in the impact on stratospheric chemistry. For example, an increase in stratospheric H_2 could lead to rising water vapour (H_2O) mixing ratios in the stratosphere, with the ultimate result of enhanced O_3 destruction (Tromp et al., 2003), although the extent to which this O_3 destruction may occur has been the subject of debate (Schultz et al., 2003; Warwick et al., 2004).

H_2 has a globally averaged tropospheric mixing ratio of approximately 530 parts per billion (ppb, 10^{-9} dry air; Novelli et al., 1999). In recent years, many studies have provided estimates for the source and sink terms in the global H_2 budget (Novelli et al., 1999; Hauglustaine and Ehhalt, 2002; Sanderson et al., 2003; Rhee et al., 2006; Price et al., 2007; Xiao et al., 2007; Ehhalt and Rohrer, 2009). We provide a range of source and sink estimates based on the above literature. Most terms are subject to considerable uncertainty, which is reflected by the large ranges. The overall source strength has been reported at 70–107 Tg a^{-1}. From this overall source term, 15–26 Tg a^{-1} originate from CH_4 oxidation, 10–18 Tg a^{-1} from the oxidation of non-methane hydrocarbons (NMHC), 11–20 Tg a^{-1} from fossil-fuels, 10–20 Tg a^{-1} from biomass burning, and 0–6 Tg a^{-1} for each of oceanic and terrestrial nitrogen (N_2) fixation processes. Microbial and enzymatic processes in soil represent the predominant sink in the overall H_2 budget (Conrad et al., 1983; Conrad and Seiler, 1985; Yonemura et al., 2000;

*Corresponding author.
Empa, Swiss Federal Laboratories for Materials Science and Technology, Laboratory for Air Pollution/Environmental Technology, Ueberlandstrasse 129, CH-8600 Duebendorf, Switzerland.
e-mail: steven.bond@empa.ch
DOI: 10.1111/j.1600-0889.2010.00509.x

Smith-Downey et al., 2006; Hammer and Levin, 2009). Soil uptake accounts for approximately three quarters (55–88 Tg a^{-1}) of the global sink strength, while oxidation through reaction with OH accounts for the remainder (15–19 Tg a^{-1}). The lifetime of H_2 in the atmosphere is ∼2 yr (Warneck, 1988; Novelli et al., 1999; Hauglustaine and Ehhalt, 2002). Novelli et al. (1999) reported a ratio of 0.97 for the Northern Hemisphere/Southern Hemisphere burden, i.e. H_2 levels that are 3% higher in the Southern Hemisphere. This is attributed to the hemispheric asymmetry of landmasses and soil sink capacity, with the Northern Hemisphere comprising 60–70% of the global land area.

The assessment of trends in tropospheric H_2 over the past decades has revealed variable results. The longest available record is reported by Grant et al. (2010), who revealed the absence of a trend in their study of continuous H_2 measurements at Mace Head over the 15-year period of 1994–2008. Other past estimates were possibly limited by the length of the available data sets, thereby leading to partly contrasting results, likely influenced by inter-annual variability. For example, in their 5-year study from 1994–1999 at Mace Head, Ireland, Simmonds et al. (2000) reported a slight upward trend of 1.2 ± 0.8 ppb a^{-1} for the Northern Hemisphere. Novelli et al. (1999) reported a slight decreasing trend in the Northern Hemisphere of 2.2 ± 0.2 ppb a^{-1} in the global marine boundary layer for the period 1991–1996. Langenfelds et al. (2002) modelled a mean global H_2 increase of 1.4 ppb a^{-1}, which is based on measurements for the period of 1992–1999. In their 5-year study from 1985–1989 covering latitudes ranging from 71.5 °N to 71.4 °S, Khalil and Rasmussen (1990) observed an increasing trend in global H_2 mixing ratios of 3.2 ± 0.5 ppb a^{-1}, which was attributed to increasing anthropogenic sources.

In this publication, continuous measurements of H_2 from August, 2005–November, 2009 at the high-altitude research station at Jungfraujoch (Switzerland) are discussed. The goal of these observations is to evaluate temporal variations in background free tropospheric H_2 conditions in the Northern Hemisphere and to identify important European source regions. Due to the prominent relationship between H_2 and carbon monoxide (CO) at the anthropogenic source, observations of CO are also addressed.

2. Methods

2.1. Measurement site

The Jungfraujoch observatory (46° 32′ N, 7° 59′ E, 3580 m a.s.l.) is a high altitude research station in the Swiss Alps, located between the peaks of Mönch (4099 m a.s.l.) to the east and of Jungfrau (4158 m a.s.l.) to the west. It is part of the Global Atmospheric Watch (GAW) program of the World Meteorological Organization (WMO) and is also part of the Swiss National Air Pollution Monitoring Network (NABEL). With its isolated and elevated position, Jungfraujoch is only periodically influenced by anthropogenic source regions. Pollution events occur primarily during frontal transport, thermally driven vertical transport (Henne et al., 2004) and southerly foehn events (Forrer et al., 2000; Reimann et al., 2004).

2.2. Gas chromatograph

H_2 and CO are measured with a gas chromatograph (GC), using a modified reduction gas analyser (RGA-3, Trace Analytical), which is controlled by Linux-based chromatography software (GCWerks, gcwerks.com). The modifications include a gas selector valve, an internal carrier gas pressure regulator, a nafion drier and a thermally insulated sample loop with a volume of ∼1 mL. The detector and column temperatures are set to 270 °C and 110 °C, respectively. Although more frequent measurements are possible, air samples are taken at 30-min intervals, bracketed by working standard measurements to calibrate the RGA-3 and to determine and correct for instrumental drift.

2.3. Quality assurance

Working standards were prepared by compressing ambient air into ∼35 L stainless steel canisters (Essex Cryogenics and Graeven Metalltechnik) using an oil-free diving compressor (RA-3, RIX Industries). These working standards—in this study ranging from 559.3–822.4 ppb H_2 and 209.5–298.0 ppb CO—were referenced against higher ranking standards and ultimately linked to the Max Planck Institute (MPI)-2009 calibration scale for H_2, which has an accuracy of 0.5% (A. Jordan, MPI Jena, personal communication, 2010) and the WMO-2000 calibration scale for CO, which has an accuracy of 1% (Novelli et al., 2003). Our Jungfraujoch measurement precision, which was derived from recurrent standard measurements, was 0.9% (1σ) for H_2 and 0.6% (1σ) for CO. Including the uncertainties from the measurements of the higher-ranking and working standards, the accuracies of our field measurements are estimated at 1.2% for H_2 and 1.3% for CO.

Quality control was also assured through participation in a round-robin intercomparison as part of the European 6th Framework Programme EuroHydros project, during which our measurements of the four intercomparison canisters (spanning 490 ppb–650 ppb) were found to be well within the uncertainty limits of those determined at the MPI Jena (home of primary scale) for the same canisters. In addition, a specific time period of our in situ RGA-3 H_2 measurements was compared with flask measurements (A. Jordan, unpublished data) taken at Jungfraujoch over the same period. The comparison did not exhibit a significant bias (mean difference between in-situ and flask measurements = 4.7 ± 8.3 ppb, $R^2 = 0.67$, $n = 28$) and results were generally in good agreement considering the constraints associated with matching the results of non-simultaneous sampling. CO measurements from this study agree well with ongoing CO measurements conducted with three other independent

instruments (R^2 ranging from 0.935 to 0.981) at Jungfraujoch (Zellweger et al., 2009).

The non-linearity of our RGA-detector was initially characterized in 2005 through the dynamic dilution of a high mixing ratio reference cylinder that contained (among some other compounds) ∼3.0 ppm H_2 and ∼1.2 ppm CO (in synthetic air). Simultaneous CH_4 measurements on a linear flame ionization detector (GC-FID) were conducted as a cross-check of the dynamic dilution. Synthetic air was used for the dilution, which was further purified to remove potential traces of H_2 and CO using a SOFNOCAT-magnesium perchlorate [$Mg(ClO_4)_2$] cartridge. Residual CH_4 was removed using a pure air generator (AADCO 737). The purified synthetic air was mixed with the high mixing ratio reference to provide 14 different H_2 and CO mixing ratios ranging from air completely free of H_2 and CO to pure high mixing ratio reference levels. Dilution ratios were set with mass flow controllers to ensure stable flow rates. These flow rates were accurately measured with a DryCal flowmeter (Bios International Corp.). CH_4, which is assumed to be linear on a GC-FID over the whole range of our experiment, was used as an independent check of the dynamic dilutions. This experiment was repeated in 2008 with slight modifications. As a cross-check during these experiments, simultaneous CO measurements with a vacuum ultraviolet resonance fluorescence instrument (Aerolaser AL5001) with linear response were used. Aliquots of these dynamic dilution mixtures were sub-sampled into stainless steel flasks and measured on the RGA at Jungfraujoch within a week of collection, serving as a second non-linearity check for this instrument. The aliquots in the stainless steel flasks were found to remain stable for at least 2 weeks following filling.

The two non-linearity experiments resulted in minor differences, which were well within the measurement precisions. For the sake of simplicity and consistency, we have therefore only applied the 2008 non-linearity results. Figure 1 depicts the variable detector sensitivity used to correct the non-linearity of the RGA-3 at Jungfraujoch as a function of the normalized height. The normalized height equals the ratio of the unknown sample peak height divided by the mean of the bracketing standard's peak height. Our experiments showed that the instrument sensitivity increases with increasing mixing ratios. For example, the normalized height sensitivity (height mol^{-1} of a sample divided by height mol^{-1} of the standard) is enhanced by approximately 10% for H_2 and 20% for CO for a sample with a peak height about double the height of a standard with mixing ratios of $H_2 \approx 640$ ppb and CO≈210 ppb.

2.4. Baseline estimation

The measurements were filtered to identify pollution events using the statistical two-dimensional Robust Extraction of Baseline Signal (2-D-REBS) filter, which extends the Robust Baseline Estimation (RBE) filter first published by Ruckstuhl et al. (2001) for baseline estimations in spectroscopic measurements and available as a package for the statistical software package R (Ruckstuhl et al., 2009). The original RBE approach is a purely statistical means of estimating the baseline from a time series that is partly influenced by recent source/sink processes (emissions, but also surface depletion). A local regression (see Loader (1999) for a textbook on local regression) is iteratively fit to the data, which successively excludes data points for the next iteration that are not within $\pm 3.5\ \sigma$ around the current fitted curve. σ is estimated from the fit residuals. Individual data points are weighted by their distance to the previous baseline fit using an asymmetric version of Tukey's bisquare robust weight function.

The two-dimensional REBS was developed for atmospheric components that show strong latitudinal gradients due to asymmetric source/sink distributions about the equator. Separating the background signal from a time series containing pollution events is an ill-posed problem and can only be solved by the RBE filter if the baseline signal varies slowly in time (mainly dominated by a seasonal cycle in the case of atmospheric trace species). However, for species showing a strong latitudinal gradient in background concentrations, rapid latitudinal transport might bring air masses to a sampling site that are not representative for the site's latitude. Such events therefore create a fast change in background concentrations that is not handled well by the RBE approach. The 2-D-REBS method provides a possibility to derive the latitudinal distribution of a trace species

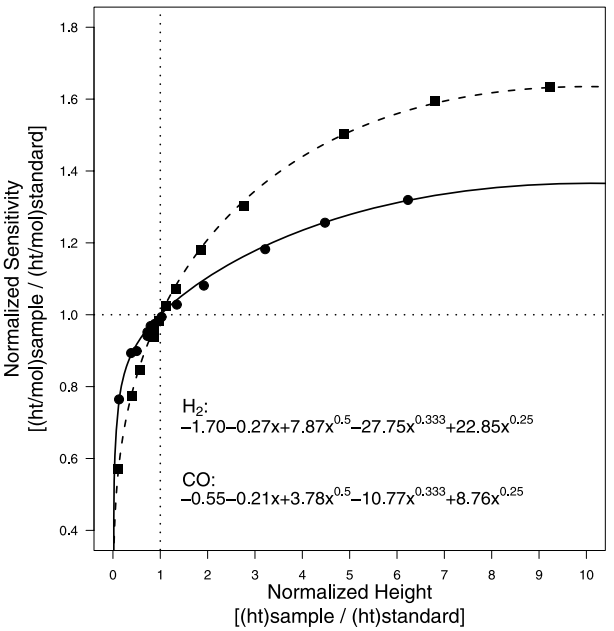

Fig. 1. Non-linearity functions for the RGA-3 at Jungfraujoch. The experimental results for H_2 (filled circles) and CO (filled squares) were fitted to the functions shown in the graph using a least-square fitting technique. Fits were forced through (1,1) to approach unity sensitivity at the normalized height of one.

background and use this information to estimate the baseline at a receptor site. Assumptions of neither the latitudinal gradient nor the source/sink distribution need to be made. In addition to standard RBE, a second explanatory variable is added to the local regression: the latitude of origin of a sampled air mass. With this, it is possible to derive a smoothed surface fit of baseline concentrations in time and latitude. For this purpose, 10-day back-trajectories were calculated using the atmospheric trajectory model FLEXTRA (Stohl et al., 1995) and European Centre for Medium-Range Weather Forecasts (ECMWF) analysis, along with 3-h forecast (T+3) wind fields with a horizontal resolution of 1° by 1° and a temporal resolution of 3 h. Trajectories were initialized every 4 h over the investigation period at the location of Jungfraujoch. The initial altitude was set to the actual station altitude, 3580 m a.s.l. The latitude of origin was then calculated from the back-trajectories. While for the original RBE, the main model parameter to be varied is the bandwidth of the local regression, there are several more parameters that have to be adjusted for the two-dimensional version. These parameters include how to estimate the air mass origin from the back-trajectories, the bandwidth of the local regression, the degree of the local polynomial and a scaling factor for the two incomparable dimensions (time and latitude) of the fit. Next to estimating a baseline time-series, the 2-D-REBS allows the estimation of latitude-time distributions of the baseline. These can be compared to other such products as derived from measurements at various locations. Here we used the National Oceanic and Atmospheric Administration (NOAA) GlobalView CO reference marine boundary layer matrix (GlobalView CO., 2009) to compare our fit results for CO and optimize our fit parameters. The comparison period was August, 2005–December, 2008. Best results in terms of correlation and residual mean square with GlobalView CO were obtained for (a) a latitude of origin as estimated as the average latitude of the trajectory 5 to 10 days before arrival at Jungfraujoch, (b) a bandwidth (local neighbourhood) according to 45 days or 2160 observations, (c) a degree of two of the local polynomial and (d) a scaling factor of 10 days degree^{-1}.

The local differences of our optimized baseline fit to the GlobalView reference marine boundary layer CO were in the range ±25 ppb. The 2-D-REBS fit for Jungfraujoch underestimated the amplitude of the annual cycle as compared to the one observed in the marine boundary layer. The latitudinal gradient was overestimated in winter with mixing ratios being too low south of 45° N, while the summer-time gradient compared well. Part of the differences could be explained by different representativeness of the measurements: global marine boundary layer air masses versus lower free tropospheric air masses mostly originating over the North Atlantic. The latitude of origin for Jungfraujoch covered a range from 10° N to 82° N. However, the data density south of 25° N and north of 65° N was rather small and therefore the uncertainties of the fit increased strongly in these areas. Between 25° N and 65° N, the standard error (95% confidence level) of the fit varies between 0.6 and 0.8 ppb for CO and between 0.4 and 0.6 for H_2. The standard deviation of the fit residuals (σ) was 11 and 9.5 for CO and H_2, respectively.

The presented method is neither limited to stations in the free troposphere nor to individual stations. The 2-D-REBS approach allows the filtering of more pollution influenced time series as well as the combination of several sites in the same regression to derive a more complete global distribution of a trace species. A detailed discussion of the method and exemplary applications are the subject of a forthcoming publication.

3. Results and discussion

3.1. Time series, seasonal cycles, trends

The H_2 and CO data sets from August, 2005–November, 2009 are shown in Fig. 2 and monthly averaged mixing ratios are listed in Table 1.

In this paper, we define 'baseline' mixing ratios as the fitted curve resulting from the 2-D-REBS filter (single points in time, black lines in Fig. 2). We define 'background' as the range of mixing ratios within 2σ (estimated from the fit residuals, see Section 2.4) from the baseline (grey band in Fig. 2) and 'pollution' and 'depletion' as the mixing ratios above and below background values, respectively. Baseline mixing ratios (Fig. 2) oscillate rapidly due to the latitudinal influence of the air mass origin (see Section 3.5). The standard deviation of half hourly baseline estimates for individual months ranged from 1 to 7 ppb. No seasonal cycle or systematic change of this oscillation was seen in the observation period. For example, baseline data for H_2 will be higher for air with its origin in the more southerly latitudes than it would be for northerly advection from the Arctic. Depletion events (i.e. points below the background measurements) are sparse for both H_2 and CO. These points represent events in which measurements were outside conditions stipulated for background conditions (2σ), likely the result of significant soil uptake. Mean baseline mixing ratios for H_2 and CO were 536 ppb and 118 ppb, respectively. Figure 3 depicts the seasonal cycle of mean baseline H_2 mixing ratios, which is characterized by an average peak-to-trough amplitude (hereafter termed amplitude) of 21 ppb, a maximum in late spring (May), and a minimum in autumn (November).

The seasonal cycle of mean baseline CO mixing ratios depicted in Fig. 3 is characterized by an amplitude of 45 ppb, a maximum in spring (March) and a minimum in autumn (October). A phase shift in the H_2 seasonal cycle of 1–2 months compared to that of CO is observed. The delayed minimum in H_2 compared to that of CO is attributed to a maximum soil H_2 sink predicted to occur later in the year due to moderately warm and dry soils in autumn (Lallo et al., 2008). The H_2 minimum in November at Jungfraujoch is delayed by ∼1 month compared to most other sites at similar latitudes (Novelli et al., 1999; Grant

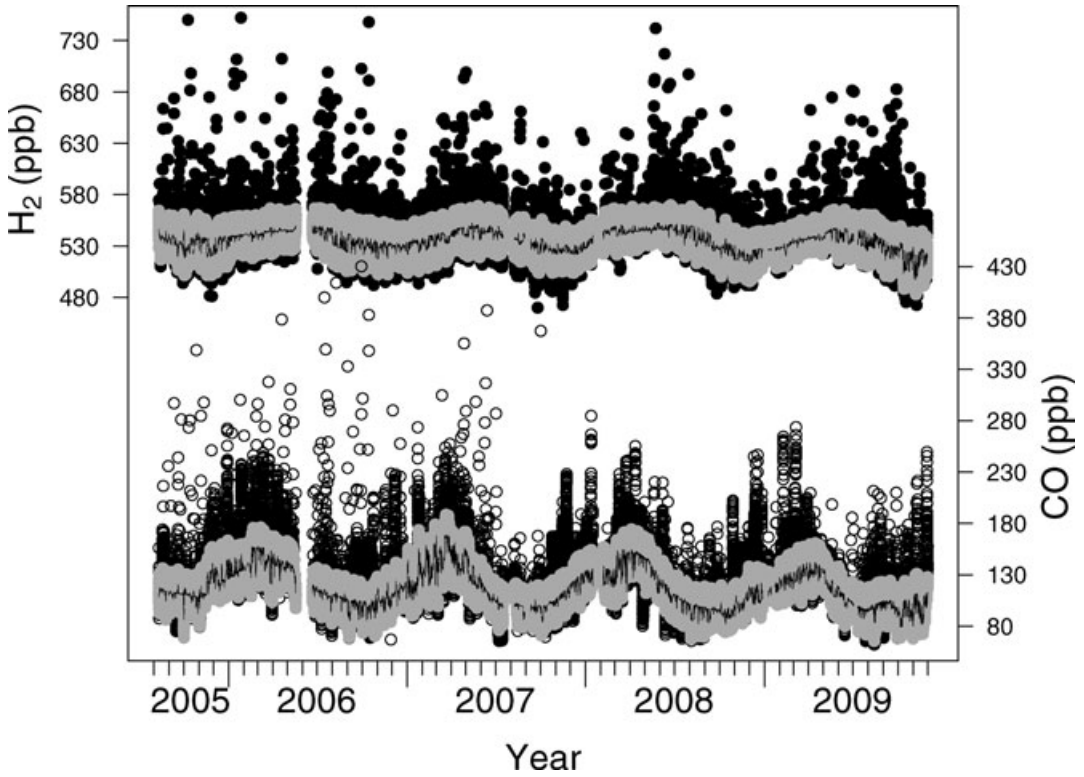

Fig. 2. H_2 (top) and CO (bottom) data sets for the period August 2005–November 2009 at Jungfraujoch. The calculated baseline fits are depicted by the black lines through the background data. Background mixing ratios (baseline fit $\pm 2\sigma$ of the fit residuals) are depicted by grey shaded areas, while pollution and depletion events border either side of the background measurements.

Table 1. Mean monthly H_2 mixing ratios at Jungfraujoch for the period August, 2005–November, 2009

Month	2005		2006		2007		2008		2009	
	All	BG	All	BG	All	BG	All	BG	All	BG
Jan	–	–	545.4	539.6	530.5	530.5	533.9	532.8	529.0	526.7
Feb	–	–	540.1	539.4	535.6	534.5	546.7	546.0	531.0	530.8
Mar	–	–	545.0	543.6	538.4	536.5	544.8	544.2	536.8	536.2
Apr	–	–	545.8	544.5	547.1	544.3	544.9	544.4	538.0	536.9
May	–	–	546.0	544.5	547.3	545.7	549.2	547.5	545.7	544.5
Jun	–	–	548.6	546.6	546.0	543.8	550.2	547.7	540.2	539.1
Jul	–	–	548.2	545.5	543.5	542.5	545.7	543.6	536.8	535.2
Aug	539.2	537.1	531.5	531.0	538.2	536.3	540.6	539.1	537.3	534.6
Sep	536.4	534.4	538.9	535.5	526.6	528.0	533.1	532.9	529.0	525.6
Oct	533.1	529.3	531.9	530.2	529.3	529.8	526.0	525.8	520.5	520.1
Nov	530.8	528.2	529.0	528.7	526.7	526.6	520.8	520.1	515.8	515.3
Dec	534.0	531.9	530.9	529.3	524.9	525.3	523.5	522.8	–	–

Notes: All mixing ratios are reported in ppb as dry-air mole fractions on the MPI-2009 calibration scale. All represents mean observations from all measurements; BG represents mean observations from background measurements.

et al., 2010), but has been similarly observed at the high-altitude Northern Hemisphere stations of Niwot Ridge (3523 m a.s.l., 40° 3′ N) and Mauna Loa (3397 m a.s.l., 19° 32′ N). We attribute this delay to the travel time of surface signals to higher altitudes in the free troposphere, particularly during the cooler months due to reduced vertical transport. Thus, air masses that have been transported to the free troposphere during the summer months (that are less depleted in H_2 due to weaker soil uptake

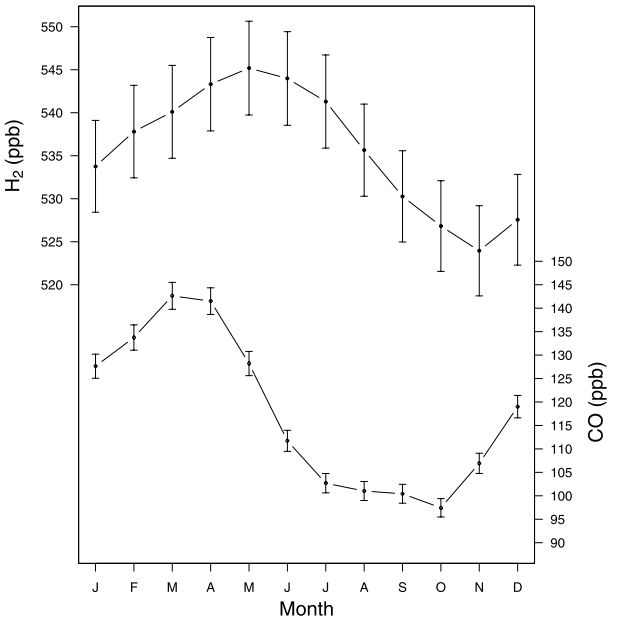

Fig. 3. Seasonal monthly mean baseline H_2 (left y-axis) and CO (right y-axis) mixing ratios at Jungfraujoch. Error bars represent expanded uncertainty at the 95% confidence level.

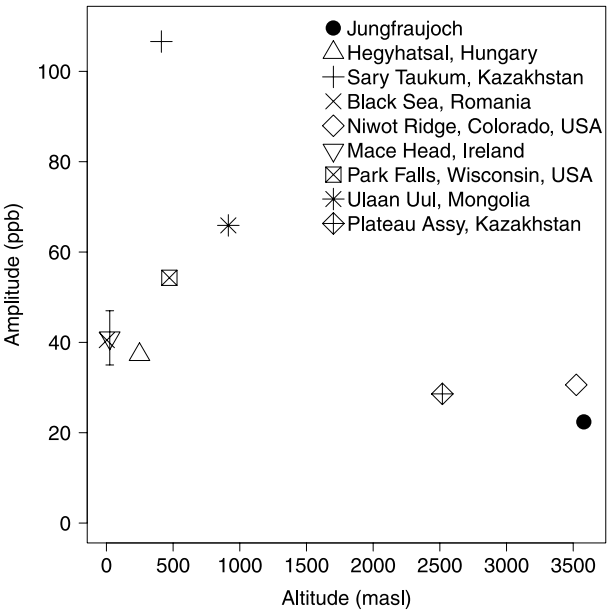

Fig. 4. H_2 seasonal amplitudes versus altitude for sites from flask measurements (http://esrl.noaa.gov) with latitudes similar to that of Jungfraujoch (46.55 ^{o}N $\pm$ 7 ^{o}N). Note that the Mace Head data point corresponds to both flask and continuous measurements, which both displayed an amplitude of 41 ppb [continuous Mace Head measurements from Grant et al. (2010)]. The error bar corresponds to the uncertainty of continuous Mace Head measurements.

and faster vertical transport) will have a prolonged influence on average mixing ratios.

The mean seasonal H_2 amplitude at Jungfraujoch is significantly smaller compared to other stations at similar latitudes. For stations within a latitude band of $\pm 7^{o}$ of Jungfraujoch, we find a general decrease in amplitude with increasing altitude. This is illustrated in Fig. 4, where Jungfraujoch measurements are compared with data from the NOAA flask sampling network (http://esrl.noaa.gov) and continuous Advanced Global Atmospheric Gases Experiment (AGAGE) observations from Mace Head (Grant et al., 2010). The amplitudes for the flask (NOAA) and continuous data (AGAGE) from Mace Head match, from which we conclude that there is no major potential bias due to differing sampling techniques, observational periods, or scales. We attribute this altitude effect to the dislocation of the major H_2 sources and sinks. With increasing altitude, the influence of the soil sink weakens and the tropospheric sources (CH_4 and NMHC oxidation) and the OH sink gain importance. Both of these major atmospheric sources, along with the atmospheric H_2 sink, are driven by OH chemistry, but the source strength is approximately double that of the sink, assuming that the ratio of the global sources and sinks also hold true for Jungfraujoch. This creates a net tropospheric source with a maximum in summer, thereby counteracting the soil sink, which in turn dominates the free tropospheric fluxes only a few months later. Such a weakening of the seasonal signal with increasing altitude has also been modelled for H_2 (Price et al., 2007). This phenomenon has also been observed for other trace gases, for which the seasonal cycle is influenced by sources and sinks located predominantly at the surface, for example CO_2 (Tanaka et al., 1983; Stephens et al., 2007).

Similarly to the work on trend measurements by Zellweger et al. (2009), we apply a linear trend model including the first four annual harmonics to remove any annual cycle from the data. This method results in a linear trend ($\pm$ standard error) of –2.04 ($\pm$0.02) ppb a^{-1} for baseline H_2 and –3.77 ($\pm$0.02) ppb a^{-1} for baseline CO results over the study period. These short-term trends observed at Jungfraujoch must be approached with caution, however, since inter-annual variation could play a role in trends derived from shorter data sets. Although the time period is too short to assess this H_2 trend in a statistical context, its similarity to trends from other data sets (Novelli et al., 1999; Simmonds et al., 2000; Grant et al., 2010) complements previous estimates, suggesting that atmospheric H_2 mixing ratios have remained relatively stable over the past couple of decades.

3.2. *Case studies*

H_2 mixing ratios at Jungfraujoch are driven by a complex interplay of (a) advection of air masses with latitudinally variable background H_2 concentrations, (b) the influence of H_2 emissions in the atmospheric boundary layer (ABL), (c) photochemical H_2 formation in the free troposphere, (d) photochemical H_2 degradation and (e) H_2 depletion by soil uptake during transport to the sampling site.

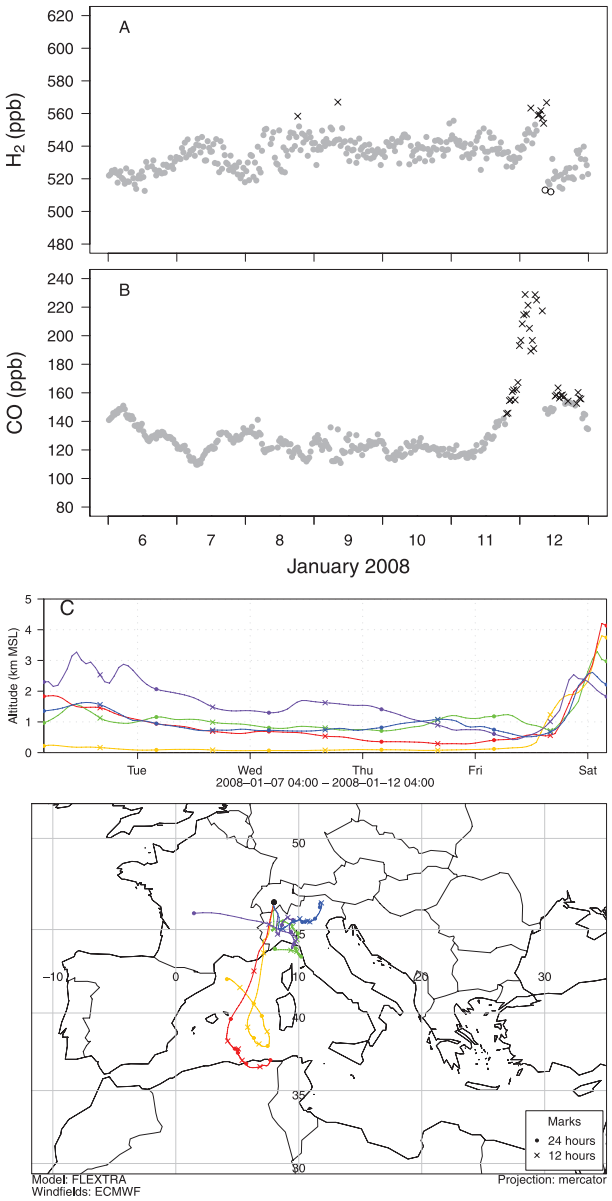

Fig. 5. Seven-day time series of H_2 (panel A) and CO (panel B) mixing ratios illustrating a pollution event on January 12, 2008. The grey filled circles correspond to background measurements, the black crosses to pollution and the black open circles to depletion measurements—all based on the 2-D-REBS filter algorithm. The corresponding 5-day backward trajectories arriving at Jungfraujoch at 0400 on January 12, 2008 are depicted in panel C. Different colours represent different arrival altitudes between 2 and 4 km a.s.l.

These conditions explain why—in contrast to measurement sites in the ABL where CO and H_2 mixing ratio time series generally show a good correlation (Steinbacher et al., 2007; Hammer et al., 2009; Yver et al., 2009)—only a small number of simultaneous pollution events for both H_2 and CO could be detected at Jungfraujoch. Figure 5 illustrates such an event, where fast advection of pollution from the nearby Po Basin (Italy) has not provided adequate time for significant deposition of H_2 to the soil during transport to Jungfraujoch. The backward trajectory analysis (panel C) confirms that the H_2 and CO pollution event on January 12, 2008 coincides with a stagnant meteorological situation where the air masses sampled at Jungfraujoch have spent several days within the European ABL prior to sweeping through the Po Valley before arrival at the measurement station. Given that pollution events from the Po Valley are observed frequently for other anthropogenic trace gases (Seibert et al., 1998; Reimann et al., 2004; Reimann et al., 2008), the relative infrequency and magnitude of such events with H_2 are presumably due to the strong soil sink.

When the situation at Jungfraujoch is more strongly driven by larger-scale advection of air masses that have spent a significant amount of time within the ABL above major land mass regions (with less distinct H_2 emissions), soil deposition begins to play an increasingly important role. Under these circumstances, events with CO pollution can be observed in the absence of H_2 pollution or even depleted H_2 mixing ratios (Fig. 6). Such situations are observed more frequently than the conditions described above, pointing to the dominance of soil uptake.

A few times per year, enhanced H_2 mixing ratios with simultaneous drops in other trace gas mixing ratios are observed when air masses originating from southern latitudes arrive at Jungfraujoch. This feature is due to the unusual above-mentioned interhemispheric H_2 distribution (Southern Hemisphere mixing ratios are larger than in the Northern Hemisphere). The most prominent example occurred on October 1, 2005, when clean maritime air masses from the southern North Atlantic reached Jungfraujoch without major land contact over Europe (Fig. 7). This pattern of reduced mixing ratios in most anthropogenic trace gases and concurrent enhancement of H_2 is unique to southerly advection. Stratospheric air mass descents to Jungfraujoch would yield depleted mixing ratios for most anthropogenic compounds. However, since H_2 varies little with altitude throughout the upper troposphere and stratosphere (Rahn et al., 2003), the enhanced H_2 mixing ratios can serve as an effective tracer for southerly advection.

3.3. *H_2 pollution events and ratios of excess H_2 to excess CO*

Periodically, anthropogenically polluted air masses reach Jungfraujoch. There is a strong seasonality in the mean ABL residence time of air masses reaching Jungfraujoch (Fig. 8). ABL residence times over the continent for the period 2005–2008 were calculated from 10-day air mass back-trajectories arriving at Jungfraujoch (FLEXTRA/ECMWF trajectories, see Section 2.4). An air mass was considered to reside in the ABL when the trajectory altitude above ground was below the climatological average ABL depth. Summer months displayed more frequent ABL contact and mean monthly residence times of up to 15

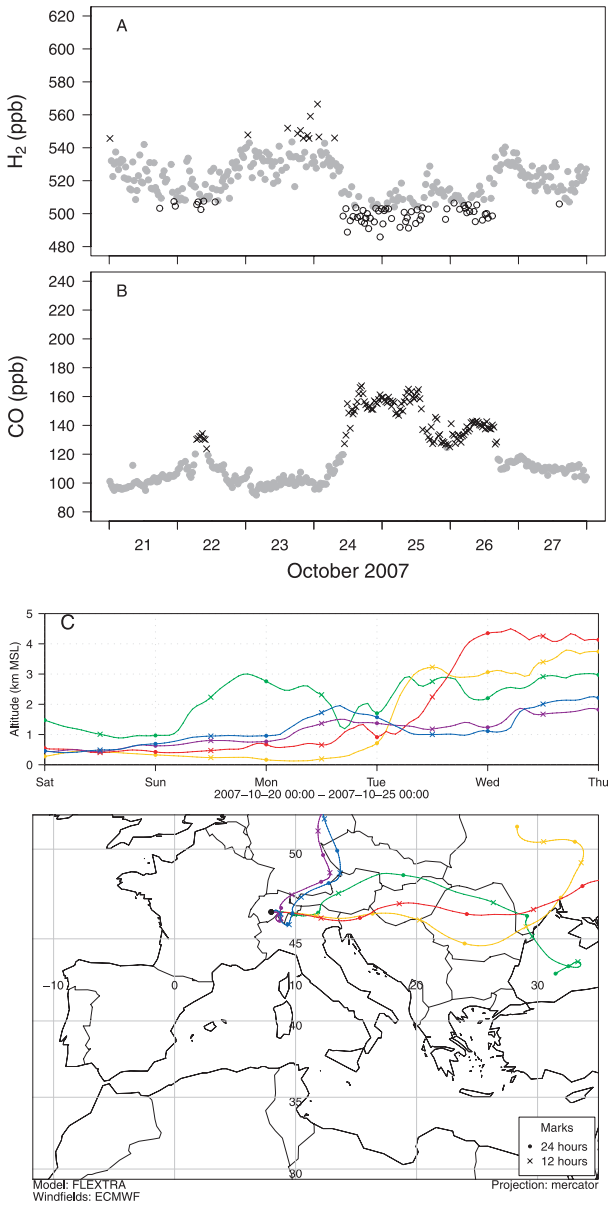

Fig. 6. Seven-day time series of H_2 (panel A) and CO (panel B) mixing ratios illustrating a CO pollution event on October 24–26, 2007 with corresponding decrease in background H_2 mixing ratios. The corresponding 5-day backward trajectories (panel C) arriving at Jungfraujoch at 0000 on October 25, 2007. See also caption of Fig. 5 for details.

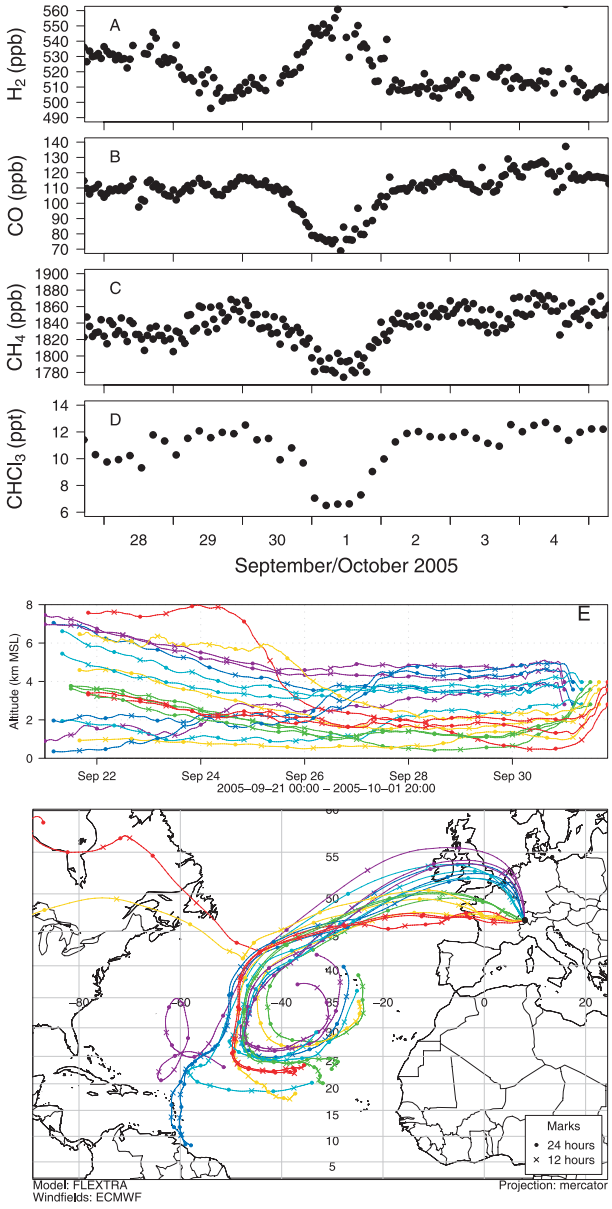

Fig. 7. Seven-day time series of H_2 (panel A), CO (panel B), CH_4 (panel C) and $CHCl_3$ (panel D) mixing ratios illustrating a depletion event for the latter gases on October 1, 2005 with simultaneous enhancement in ambient H_2. Panel E illustrates the corresponding 10-day backward trajectories arriving at Jungfraujoch on October 1, 2005. Different colours represent different arrival altitudes and times.

h in the ABL, three to four times as much as in the winter months when ABL contacts were infrequent (below 20%). In addition, vertical transport of ABL air in thermally-induced circulations that are not fully captured by the trajectory calculations are more frequent in summer (Zellweger et al., 2003; Henne et al., 2005), further increasing the seasonal contrast between ABL influenced observations in summer and free tropospheric conditions in winter. With longer residence times close to the surface allowing an enhanced loading of H_2 and CO pollution, these processes alone would suggest that the summer months should show the most frequent and also the strongest pollution events at Jungfraujoch. For H_2, we do indeed find the highest frequency of pollution events in the summer months (with the exception of January due to an exceptionally high number of pollution events during that month in 2006). However, there is no pronounced seasonality

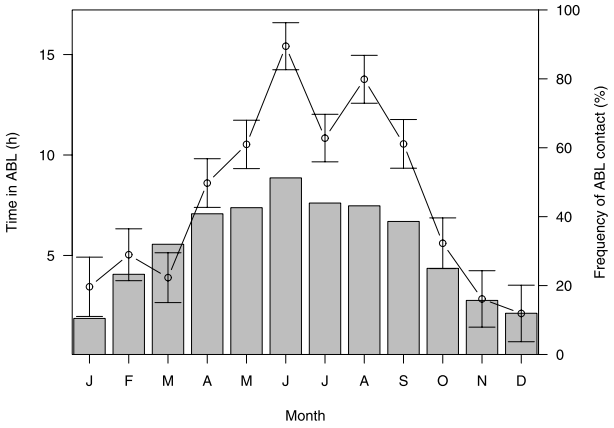

Fig. 8. Monthly mean (line referring to left y-axis) and its 95% confidence levels (error-bars; log-normal statistics) of atmospheric boundary layer (ABL) residence times calculated from 10-day back trajectories arriving at Jungfraujoch (3580 m a.s.l.). Bars (right y-axis) give the frequency of ABL influenced trajectories.

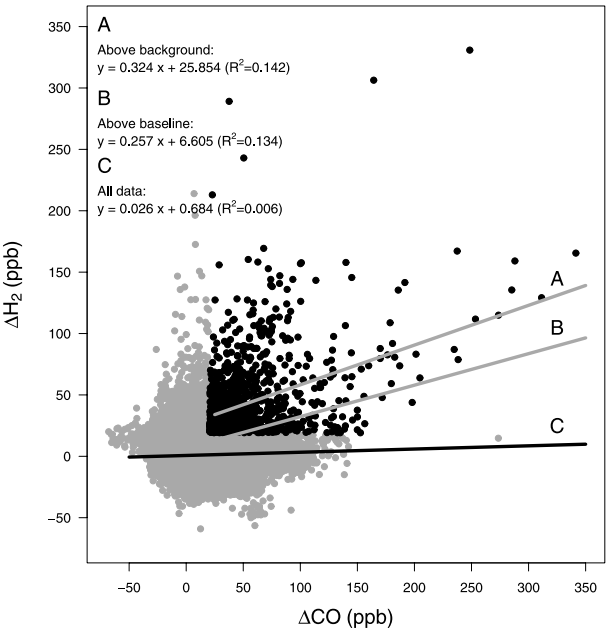

Fig. 9. Excess (mixing ratio minus corresponding baseline value) H_2 (ΔH_2) and CO (ΔCO) for Jungfraujoch. The black filled circles correspond to the above-background (pollution) data. Linear regressions are shown as solid lines.

in the magnitude of the H_2 pollution events. We speculate that the strong soil sink may be responsible for the lack of large-magnitude pollution events and that there is a resulting compensatory source–sink effect in the ABL. After assessing the H_2 and CO pollution characteristics at Jungfraujoch more quantitatively in the next paragraphs, we will then provide a rough calculation in Section 3.4 to support this speculation.

Combined investigation of H_2 and CO pollution helps to understand their common sources (e.g. gasoline traffic combustion) and to upscale H_2 emissions against much better known CO emission inventories. For our discussion of pollution, we define excess H_2 (ΔH_2) as the H_2 mixing ratio minus the corresponding baseline value. We define excess CO (ΔCO) analogously. For measurements in urban and suburban areas, the $\Delta H_2/\Delta$CO is dominated by that of gasoline engine exhaust (Bond et al., 2010; Vollmer et al., 2010). These ratios have typically displayed a range of ~0.3–0.5 (Steinbacher et al., 2007; Vollmer et al., 2007; Aalto et al., 2009; Hammer et al., 2009; Yver et al., 2009). For remote stations such as Mace Head, the $\Delta H_2/\Delta$CO is much lower at 0.15–0.18 (Simmonds et al., 2000; Grant et al., 2010) and the extraction of the anthropogenic $\Delta H_2/\Delta$CO source signature is more difficult. For Jungfraujoch, we have also investigated the $\Delta H_2/\Delta$CO relationship since it might allow retrieving representative numbers for aggregated sources over large parts of Central Europe due to the huge footprint observed at Jungfraujoch. Our results must be treated with caution because they depend significantly on the data selections and the type of fitting routine. We have ultimately chosen a least-squares fitting technique, fitexy (Press et al., 1992), which takes the uncertainties of both H_2 and CO data into account. Had we chosen to use a standard linear regression, too much weight would have been put on the high-end extreme values, which would have had too much influence on the slope of the curve and thus led to less representative results.

We find $\Delta H_2/\Delta$CO to be 0.324 ± 0.005 ($R^2 = 0.142$) when choosing above-background data (black filled circles in Fig. 9). Note that for this calculation, only data when both H_2 and CO are above the grey band in Fig. 2 (baseline plus 2σ) are selected, but the Δ-values used are the differences of the measured values from the baseline fit. This data selection depends on the width of the background data set and also a priori excludes data for which one of the two compounds in not elevated (e.g. depleted H_2). This $\Delta H_2/\Delta$CO (~1140 data points) is similar to urban measurements, presumably because the data selection process limits the data set to pollution events that are likely derived from air masses rapidly transported to Jungfraujoch without significant H_2 soil removal or mixing with background air (hence the elevated values). The poor correlation between ΔH_2 and ΔCO ($R^2 = 0.142$) and the relatively high y-axis intercept (~26 ppb) illustrate that this $\Delta H_2/\Delta$CO ratio must be interpreted with caution.

If we select all above-baseline data, then our $\Delta H_2/\Delta$CO is 0.257 ± 0.002 ($R^2 = 0.134$). This relationship also captures the enhanced events of both H_2 and CO that were not classified as pollution events, but within the upper half of the background band. If we choose the entire data set, then $\Delta H_2/\Delta$CO is 0.026 ± 0.001 with essentially no correlation between the two trace gases ($R^2 = 0.006$). Nevertheless, these results qualitatively confirm the decreasing $\Delta H_2/\Delta$CO ratio with increasing distance from the anthropogenic source, but also show the difficulties and dependencies on the data selection for such ratios (Fig. 9). The lack of a correlation between ΔH_2 and ΔCO is

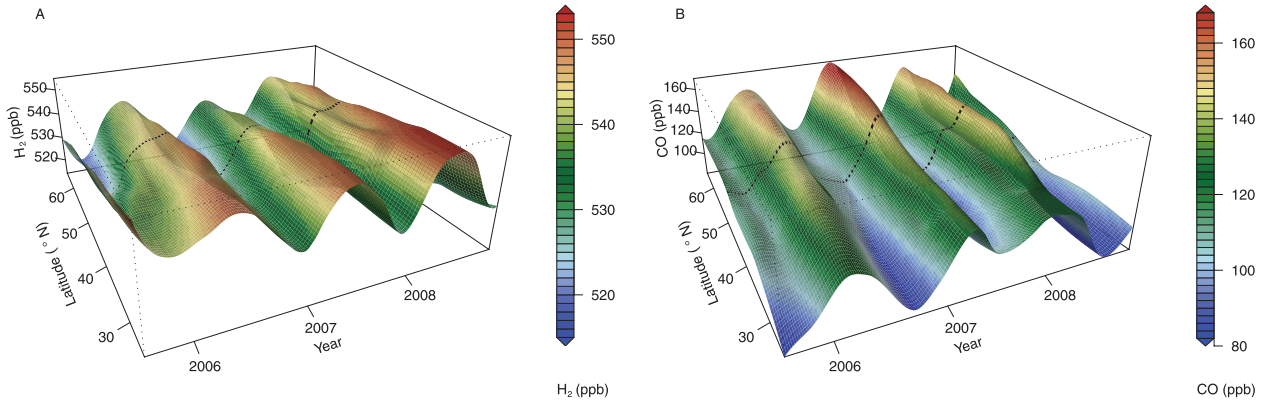

Fig. 10. Latitudinal dependence of H_2 and CO using the graphical 2-D-REBS method, illustrating the results of trajectory analysis for the origin of H_2 (panel A) and CO (panel B). Clearly visible is the origin of low-northern latitudes for the highest H_2 mixing ratios, while mid- to high-northern latitudes are responsible for the highest CO mixing ratios. The latitude of Jungfraujoch (46 °N) is represented by the dashed black line. The colour bar on the right of each diagram represents atmospheric mixing ratios of both H_2 and CO.

attributed to variable H_2 removal by soil. A rough estimate for this removal process is provided in the following sub-section.

3.4. *Soil uptake assessment*

A method involving 222-radon measurements has recently been proposed to remove the influence of the soil sink from the $\Delta H_2/\Delta CO$ ratio in urban/sub-urban areas (Hammer et al., 2009). This method cannot be applied to our Jungfraujoch data due to the lack of 222-radon measurements at Jungfraujoch and the lack of a correlation in the observed $\Delta H_2/\Delta CO$. To evaluate the possible influence of H_2 soil deposition on the H_2 mixing ratios during transport to Jungfraujoch we make a rough calculation that aims at assessing the magnitude of the H_2 removal by soil during the warmer and dryer months. We consider an initial air mass with a characteristic molar $\Delta H_2/\Delta CO$ ratio of 0.45–0.48 in polluted environments (Hammer et al., 2009). We assume typical transport times to Jungfraujoch of 8 h, an up-valley wind layer height of 100 m (Henne et al., 2004), negligible CO deposition, a H_2 deposition velocity of 1×10^{-4} m s^{-1} and background conditions of 520 ppb and 90 ppb for H_2 and CO, respectively. Based on these assumptions we find a $\Delta H_2/\Delta CO$ of 0.35–0.38 upon arrival at Jungfraujoch. This ratio is only slightly higher than the observed $\Delta H_2/\Delta CO$ of 0.324 ± 0.005 (see Section 3.3) for polluted air masses. However, given the uncertainties in our assumptions, it suggests that soil deposition can explain the observed ratios at Jungfraujoch. Other processes such as photochemistry during transport or entrainment of air masses might also influence the $\Delta H_2/\Delta CO$ at Jungfraujoch.

The key role of soil deposition also becomes visible when looking at the residence times in the boundary layer for the different sub-sets of the H_2 data (pollution, background, depletion). Whereas the median residence time in the boundary layer within the last 96 h before arrival at Jungfraujoch for the whole data set is 12.8 h, the residence times of the sub-sets for pollution, background and depletion are 10.3 h, 12.7 h and 35.3 h, respectively. This indicates that a strong boundary layer influence favours low H_2 mixing ratios in contrast to most of the other trace gases observed at the high-Alpine site. A similar, but more regional approach to distinguish prevailing residence times in regions close to Jungfraujoch and more distant regions was not possible due to limited statistics.

3.5. *Latitudinal dependency of background H_2 mixing ratios*

A co-benefit of the background determination with consideration of the air mass origin—that is the mean latitude of the air mass 5–10 days before arrival at Jungfraujoch—is the information about the latitudinal dependence of background H_2 and CO. Thus, the 2-D-REBS method allows for graphical display of the latitudinal dependence of H_2 and CO at a single station (Fig. 10), in contrast to multi-station approaches as they are reported for other trace gases by the World Data Centre for Greenhouse Gases (JMA and WMO, 2009) or GlobalView CO (2009). The dependence of H_2 on latitude is distinct, with highest mixing ratios originating from more southerly latitudes. At ∼40–60 °N, a slight trough is observed in H_2 levels. This can be attributed to the active soil sink at these latitudes, which is much less pronounced outside this latitude band due to decreasing source strength and land mass area optimally suited for H_2 uptake by soils. This same north–south gradient was observed by Novelli et al. (1999) in their global H_2 assessment. In that study, the latitudinal gradient equated to an approximately 30 ppb decrease between the latitudes of 20 °N and 60 °N. According to our study, the gradient from 20–60 °N is ∼20 ppb (Fig. 10A). For CO, the well-known opposite latitudinal gradient compared to H_2 is visible in Fig. 10B. Our approach shows considerably

smaller annual amplitudes than the GlobalView CO product and a general overestimation of the latitudinal gradient in winter, as has already been highlighted in Section 2.4. The main reason for these differences can be seen in the different air masses taken into account in the fit. Here we use (unpolluted) samples that are more representative of the lower free troposphere over the North Atlantic and Western Europe, while GlobalView CO is derived from (unpolluted) samples in the marine boundary layer. The agreement was not as good during the winter months, indicating a stronger decoupling between surface air and lower free troposphere, when compared with the summer months.

4. Conclusion

This paper provides a first insight into the characterization of atmospheric molecular H_2 in a primarily free tropospheric context, along with the key processes determining the free tropospheric mixing ratios. Highest background H_2 mixing ratios were observed in May, while the lowest were observed in November. The seasonal minimum in November was delayed compared with other stations at similar latitudes and the peak-trough amplitude of 21 ppb was comparatively less pronounced than that of lower elevation sites. These differences suggest that a dampening and delay of the surface soil sink signal occur during its vertical propagation to the free troposphere and that the delay and decreasing peak-trough amplitude become more pronounced through a combination of increasing distance from the source and greater vertical transport time. Further research in these areas at both high and low altitude observatories would help to further develop this hypothesis.

Our specific case studies have revealed that H_2 mixing ratios at Jungfraujoch are influenced by a number of factors including advection of air masses with latitudinally variable background H_2 concentrations, the influence of H_2 emissions in the ABL and H_2 depletion by soil uptake during transport to the sampling site. Measurements of $\Delta H_2/\Delta CO$ at Jungfraujoch often reveal lower ratios compared to the $\sim$0.5 from traffic combustion studies (Vollmer et al., 2007), a discrepancy most likely caused by a compensatory effect between pollution and the strong H_2 soil sink. The largest of these compensatory effects occur in summer when air masses have longest contact with the ABL before reaching Jungfraujoch. At that time, pollution is strongest, but so is the soil sink. A simple box model calculation revealed that soil uptake can largely explain the small $\Delta H_2/\Delta CO$ ratios at Jungfraujoch compared to ratios observed at less remote sites.

The present study has shown that Jungfraujoch is a favourable location (central Europe) for studying H_2 in the free troposphere. The suitability of the site allows the investigation of transport processes from the ABL to the free troposphere, along with free tropospheric transport and their effects on H_2 mixing ratios. The lengthening of the time series into the future will allow more reliable trend estimates and enable the investigation of effects of a more H_2-intensive economy, including the amount of time for the atmospheric system to respond to disturbances (e.g. increased emissions) of the current source–sink equilibrium. Future trend analysis at Jungfraujoch could therefore serve as a robust indicator for assessing the behaviour of H_2 as the fraction of mobile- and stationary-based H_2 applications increases. This study has illustrated some of the advantages of continuous measurements. Whereas flask sampling is an appropriate approach for evaluating trends and the influence of increasing H_2-based applications on baseline mixing ratios, continuous measurements provide an extended benefit when features such as specific sources, sinks and transport phenomena are of interest.

5. Acknowledgments

The authors would like to thank the International Foundation High Altitude Research Stations Jungfraujoch and Gornergrat (HFSJG) for access to the Jungfraujoch facilities, and the custodians at Jungfraujoch—the families Fischer, Seiler and Hemund—for their assistance at the research station. The authors also acknowledge the use of H_2 data from the National Oceanic and Atmospheric Administration's Earth System Research Laboratory-Global Monitoring Division (NOAA/ESRL-GMD) cooperative air sampling network. Christoph Zellweger is acknowledged for his contributions regarding the quality assurance of the CO measurements. Peter Salameh is acknowledged for his help with the GCWerks software and advice on correcting RGA non-linearity. Funding was provided by the European Union framework program FP6-2005-Global-4 'EuroHydros' and the 'Competence Center for Energy and Mobility, Switzerland (CCEM-CH)'.

References

Aalto, T., Lallo, M., Hatakka, J. and Laurila, T. 2009. Atmospheric hydrogen variations and traffic emissions at an urban site in Finland. *Atm. Chem. Phys.* **9**, 7387–7396.

Bond, S. W., Alvarez, R., Vollmer, M. K., Steinbacher, M., Weilenmann, M. and co-authors. 2010. Molecular hydrogen (H_2) emissions from gasoline and diesel vehicles. *Sci. Total Environ.* **408**, 3596–3606.

Conrad, R. and Seiler, W. 1985. Influence of temperature, moisture, and organic carbon on the flux of H_2 and CO between soil and atmosphere: field studies in subtropical regions. *J. Geophys. Res.* **90**, 5699–5709.

Conrad, R., Weber, M. and Seiler, W. 1983. Kinetics and electron transport of soil hydrogenases catalyzing the oxidation of atmospheric hydrogen. *Soil Biol. Biochem.* **15**, 167–173.

Derwent, R. G., Simmonds, P., O'Doherty, S., Manning, A., Collins, W. and co-authors. 2006. Global environmental impacts of the hydrogen economy. *Int. J. Nucl. Hydrog. Prod. Appl.* **1**, 57–67.

Ehhalt, D. H. and Rohrer, F. 2009. The tropospheric cycle of H_2: a critical review. *Tellus B* **61**, 500–535.

Forrer, J., Rüttimann, R., Schneiter, D., Fischer, A., Buchmann, B. and co-authors. 2000. Variability of trace gases at the high-Alpine site Jungfraujoch caused by meteorological transport processes. *J. Geophys. Res.* **105**, 12 241–12 251.

GlobalView, CO. 2009. Cooperative atmospheric data integration project–carbon monoxide. *Available at: Internet via anonymous FTP to ftp.cmdl.noaa.gov, Path: ccg/co/GLOBALVIEW* (Last accessed 10 April 2010).

Grant, A., Witham, C. S., Simmonds, P. G., Manning, A. J. and O'Doherty, S. 2010. A 15 year record of high-frequency, in situ measurements of hydrogen at Mace Head, Ireland. *Atmos. Chem. Phys.* **10**, 1203–1214.

Hammer, S. and Levin, I. 2009. Seasonal variation of the molecular hydrogen uptake by soils inferred from continuous atmospheric observations in Heidelberg, southwest Germany. *Tellus* **61B**, 556–565.

Hammer, S., Vogel, F., Kaul, M. and Levin, I. 2009. The H_2/CO ratio of emissions from combustion sources: comparison of top-down with bottom-up measurements in southwest Germany. *Tellus* **61B**, 547–555.

Hauglustaine, D. A. and Ehhalt, D. H. 2002. A three-dimensional model of molecular hydrogen in the troposphere. *J. Geophys. Res.* **107**, 4330, doi:10.1029/2001JD001156.

Henne, S., Furger, M., Nyeki, S., Steinbacher, M., Neininger, B. and co-authors. 2004. Quantification of topographic venting of boundary layer air to the free troposphere. *Atmos. Chem. Phys.* **4**, 497–509.

Henne, S., Furger, M. and Prévôt, A. S. H. 2005. Climatology of mountain venting-induced elevated moisture layers in the lee of the Alps. *J. Appl. Meteorology* **44**, 620–633.

JMA and WMO. 2009. WMO World Data Centre for Greenhouse Gases (WDCGG) Data Summary GAW Data Volume IV, Greenhouse Gases and Other Atmospheric Gases. Japan Meteorological Agency and World Meteorological Organization. 105pp.

Khalil, M. A. K. and Rasmussen, R. A. 1990. Global increase in atmospheric molecular hydrogen. *Nature* **347**, 743–745.

Lallo, M., Aalto, T., Laurila, T. and Hatakka, J. 2008. Seasonal variations in hydrogen deposition to boreal forest soil in southern Finland. *Geophys. Res. Lett.* **35**, doi:10.1029/2007GL032357.

Langenfelds, R. L., Francey, R. J., Pak, B. C., Steele, L. P., Lloyd, J. and co-authors. 2002. Interannual growth rate variations of atmospheric CO_2 and its $\delta^{13}C$, H_2, CH_4, and CO between 1992 and 1999 linked to biomass burning. *Global Biogeochem. Cycles* **16**, 1048, doi:10.1029/2001GB001466.

Loader, C. 1999. *Local Regression and Likelihood*. Springer, New York, 290pp.

Novelli, P. C., Lang, P. M., Masarie, K. A., Hurst, D. F., Myers, R. and co-authors. 1999. Molecular hydrogen in the troposphere: global distribution and budget. *J. Geophys. Res.* **104**, 30 427–30 444.

Novelli, P. C., Masarie, K. A., Lang, P. M., Hall, B. D., Myers, R. C. and co-authors. 2003. Reanalysis of tropospheric CO trends: effects of the 1997–1998 wildfires. *J. Geophys. Res.* **108**, doi:1029/2002JD003031.

Press, W. H., Vetterling, W. T. and Flannery, B. P., 1992. Numerical recipes in C, The art of scientific computing. Cambridge University Press, Cambridge, U.K., 994pp.

Price, H., Jaeglé, L., Rice, A., Quay, P., Novelli, P. C. and co-authors. 2007. Global budget of molecular hydrogen and its deuterium content: constraints from ground station, cruise, and aircraft observations. *J. Geophys. Res.* **112**, doi:10.1029/2006JD008152.

Rahn, T., Eiler, J. M., Boering, K. A., Wennberg, P. O., McCarthy, M. C. and co-authors. 2003. Extreme deuterium enrichment in stratospheric hydrogen and the global atmospheric budget of H_2. *Nature* **424**, 918–921.

Reimann, S., Schaub, D., Stemmler, K., Folini, D., Hill, M. and co-authors. 2004. Halogenated greenhouse gases at the Swiss High Alpine Site of Jungfraujoch (3580 m asl): continuous measurements and their use for regional European source allocation. *J. Geophys. Res.* **109**, doi:10.1029/2003JD003923.

Reimann, S., Vollmer, M. K., Folini, D., Steinbacher, M., Hill, M. and co-authors. 2008. Observations of long-lived anthropogenic halocarbons at the high-Alpine site of Jungfraujoch (Switzerland) for assessment of trends and European sources. *Sci. Total Environ.* **391**, 224–231.

Rhee, T. S., Brenninkmeijer, C. A. M. and Röckmann, T. 2006. The overwhelming role of soils in the global atmospheric hydrogen cycle. *Atmos. Chem. Phys.* **6**, 1611–1625.

Ruckstuhl, A., Unternaehrer, T. and Locher, R. 2009. R: IDPmisc: Utilities of Institute of Data Analyses and Process Design. Available at: www.idp.zhaw.ch, http://CRAN.R-project.org/package=IDPmisc, R package version 1.1.06, 2009 (Last accessed 15 July 2010).

Ruckstuhl, A. F., Jacobson, M. P., Field, R. W. and Dodd, J. A. 2001. Baseline subtraction using robust local regression estimation. *J. Quant. Spectrosc. Radiat. Transfer* **68**, 179–193.

Sanderson, M. G., Collins, W. J., Derwent, R. G. and Johnson, C. E. 2003. Simulation of global hydrogen levels using a Lagrangian three-dimensional model. *J. Atmos. Chem.* **46**, 15–28.

Schultz, M. G., Diehl, T., Brasseur, G. P. and Zittel, W. 2003. Air pollution and climate-forcing impacts of a global hydrogen economy. *Science* **302**, 624–627.

Seibert, P., Kromp-Kolb, H., Kasper, A., Kalina, M., Puxbaum, H. and co-authors. 1998. Transport of polluted boundary layer air from the Po Valley to high-alpine sites. *Atmos. Environ.* **32**, 3953–3965.

Simmonds, P. G., Derwent, R. G., O'Doherty, S., Ryall, D. B., Steele, L. P. and co-authors. 2000. Continuous high-frequency observations of hydrogen at the Mace Head baseline atmospheric monitoring station over the 1994–1998 period. *J. Geophys. Res.* **105**, 12 105–12 121.

Smith-Downey, N. V., Randerson, J. T. and Eiler, J. M. 2006. Temperature and moisture dependence of soil H_2 uptake measured in the laboratory. *Geophys. Res. Lett.* **33**, doi:10.1029/2006GL026749.

Steinbacher, M., Fischer, A., Vollmer, M. K., Buchmann, B., Reimann, S. and co-authors. 2007. Perennial observations of molecular hydrogen (H_2) at a suburban site in Switzerland. *Atmos. Environ.* **41**, 2111–2124.

Stephens, B. B., Gurney, K. R., Tans, P. P., Sweeney, C., Peters, W. and co-authors. 2007. Weak northern and strong tropical land carbon uptake from vertical profiles of atmospheric CO_2. *Science* **316**, 1732–1735.

Stohl, A., Wotawa, G., Seibert, P. and Kromp-Kolb, H. 1995. Interpolation errors in wind fields as a function of spatial and temporal resolution and their impact on different types of kinematic trajectories. *J. Appl. Meteorol.* **34**, 2149–2165.

Tanaka, M., Nakazawa, T. and Aoki, S. 1983. Concentration of atmospheric carbon dioxide over Japan. *J. Geophys. Res.* **88**, 1339–1344.

Tromp, T., Shia, R., Allen, M., Eiler, J. M. and Yung, Y. L. 2003. Potential environmental impact of a hydrogen economy on the stratosphere. *Science* **300**, 1740–1742.

Vollmer, M. K., Juergens, N., Steinbacher, M., Reimann, S., Weilenmann, M. and co-authors. 2007. Road vehicle emissions of molecular hydrogen (H_2) from a tunnel study. *Atmos. Environ.* **41**, 8355–8369.

Vollmer, M. K., Walter, S., Bond, S. W., Soltic, P. and Röckmann, T. 2010. Molecular hydrogen (H_2) emissions and their isotopic signatures (H/D) from a motor vehicle: implications on atmospheric H_2. *Atmos. Chem. Phys.* **10**, 5707–5718.

Warneck, P., 1988. Chemistry of the natural atmosphere. Academic Press, Inc., San Diego, 927pp.

Warwick, N. J., Bekki, S., Nisbet, E. G. and Pyle, J. A. 2004. Impact of a hydrogen economy on the stratosphere and troposphere studied in a 2-D model. *Geophys. Res. Lett.* **31**, doi:10.1029/2003GL019224.

Xiao, X., Prinn, R. G., Simmonds, P. G., Steele, L. P., Novelli, P. C. and co-authors. 2007. Optimal estimation of the soil uptake rate of molecular hydrogen from the Advanced Global Atmospheric Gases Experiment and other measurements. *J. Geophys. Res.* **112**, doi:10.1029/2006JD007241.

Yonemura, S., Yokozawa, M., Kawashima, S. and Tsuruta, H. 2000. Model analysis of the influence of gas diffusivity in soil on CO and H_2 uptake. *Tellus* **52B**, 919–933.

Yver, C., Schmidt, M., Bousquet, P., Zahorowski, W. and Ramonet, M. 2009. Estimation of the molecular hydrogen soil uptake and traffic emissions at a suburban site near Paris through hydrogen, carbon monoxide and radon-222 semi-continuous measurements. *J. Geophys. Res.* **114**, doi:10.1029/2009JD012122.

Zellweger, C., Forrer, J., Hofer, P., Nyeki, S., Schwarzenbach, B. and co-authors. 2003. Partitioning of reactive nitrogen (NO_y) and dependence on meteorological conditions in the lower free troposphere. *Atmos. Chem. Phys.* **3**, 779–796.

Zellweger, C., Hüglin, C., Klausen, J., Steinbacher, M., Vollmer, M. K. and co-authors. 2009. Inter-comparison of four different carbon monoxide measurements techniques and evaluation of the long-term carbon monoxide time series of Jungfraujoch. *Atmos. Chem. Phys.* **9**, 3491–3503.